Electronic Supplemental Information for

Expanding Pore Sizes of ZIF-8-Derived Nitrogen-Doped Microporous Carbon via C_{60} Embedding: toward Improved Anode Performance for Lithium-Ion Battery

Jian Guan,[a] *Xiongwu Zhong,*[b] *Xiang Chen,*[a] *Xianjun Zhu,*[a] *Panlong Li,*[a] *Jianhua Wu,*[a] *Yalin Lu,*[a] *Yan Yu,**[b] *and Shangfeng Yang**[a]

[a] Hefei National Laboratory for Physical Sciences at Microscale, Key Laboratory of Materials for Energy Conversion, Chinese Academy of Sciences, Department of Materials Science and Engineering, Synergetic Innovation Center of Quantum Information & Quantum Physics, University of Science and Technology of China, Hefei 230026, China

[b] Key Laboratory of Materials for Energy Conversion, Chinese Academy of Sciences, Department of Materials Science and Engineering, University of Science and Technology of China, Hefei 230026, China

E-mail: sfyang@ustc.edu.cn (S. Y.); yanyumse@ustc.edu.cn (Y. Y.)

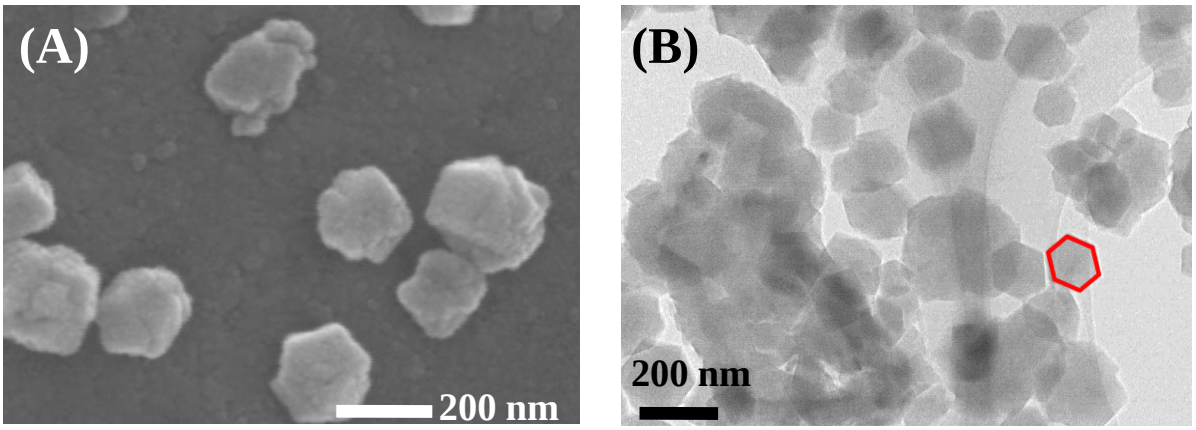

Figure S1. SEM (A) and TEM (B) images of the unmodified ZIF-8. The average particle size of ZIF-8 nanocrystals is ~200 nm according to both SEM and TEM images. Besides, ZIF-8 nanoparticles exhibit 6-fold symmetry according to the TEM image (marked by the red hexagon), in agreement with that reported in literatures.[S1]

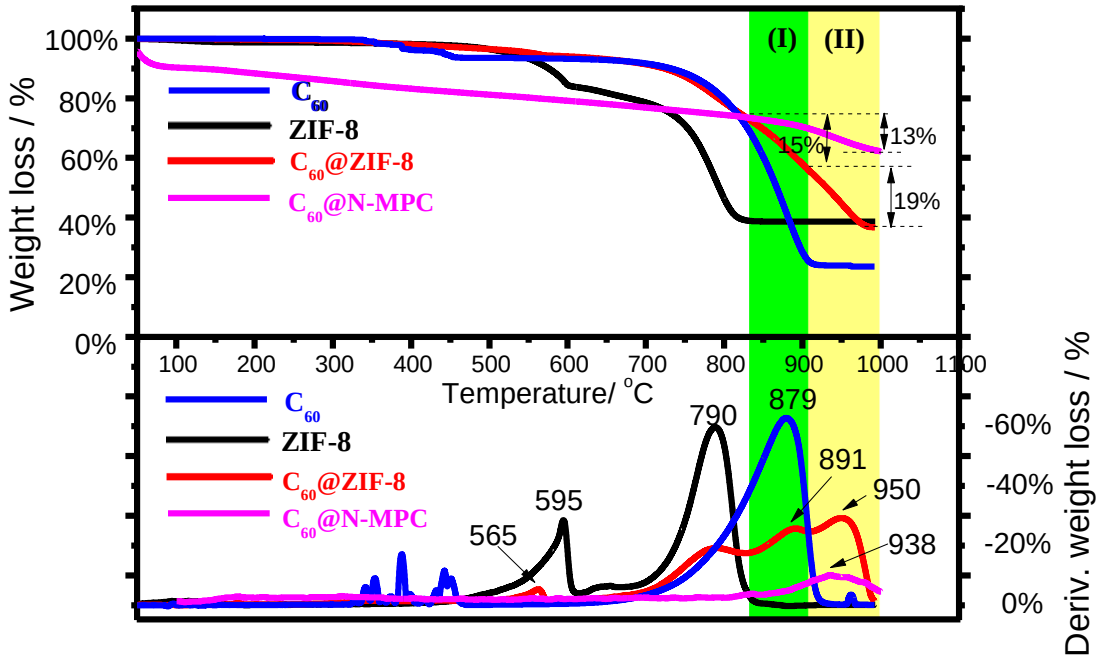

Figure S2. Thermogravimetric analysis (TGA, top) and derivative thermogravimetric (DTG, down) curves of of C_{60}, ZIF-8, C_{60}@ZIF-8 and C_{60}@N-MPC. The heating rate is 5 °C/min. According to the final weight-loss step attributed to the thermal detaching of the embedded C_{60} moiety (~15 wt% and 13% wt% for C_{60}@ZIF-8 and C_{60}@N-MPC, respectively), the average molar content of C_{60} molecule within C_{60}@ZIF-8/C_{60}@N-MPC can be estimated to be 2.8/2.5 per 1000 carbon atoms.

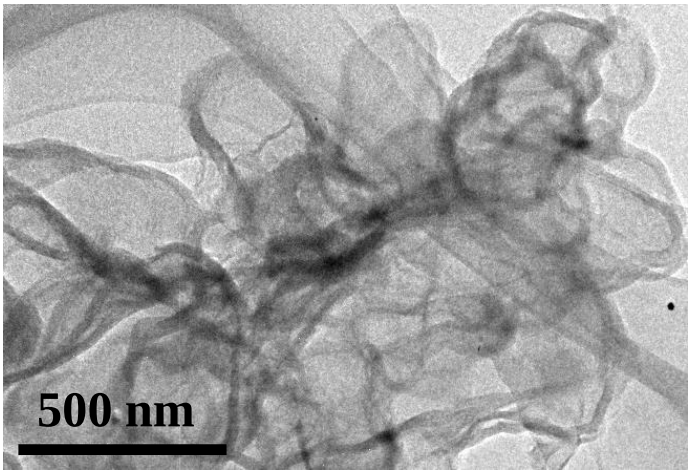

Figure S3. TEM image of the unmodified N-MPC.

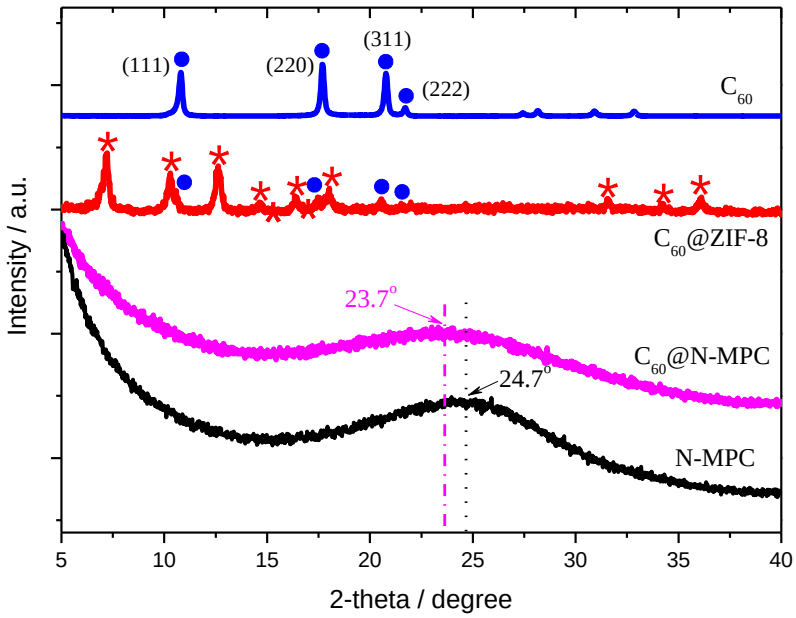

Figure S4. XRD patterns of C_{60}, C_{60}@ZIF-8, C_{60}@N-MPC and N-MPC. The filled circles label the signals of C_{60}, and the asterisks mark the diffraction signals of ZIF-8. According to the broad diffraction peak centered at ca. 24.7° observed in the XRD diffraction pattern of N-MPC, a layer-to-layer *d*-spacing of 0.372 nm is calculated for N-MPC. This peak slightly downshifts to ca. 23.7° in the XRD pattern of C_{60}@N-MPC, suggesting the increase of the layer-to-layer *d*-spacing of graphite layers likely due to the intercalation of C_{60} molecules.

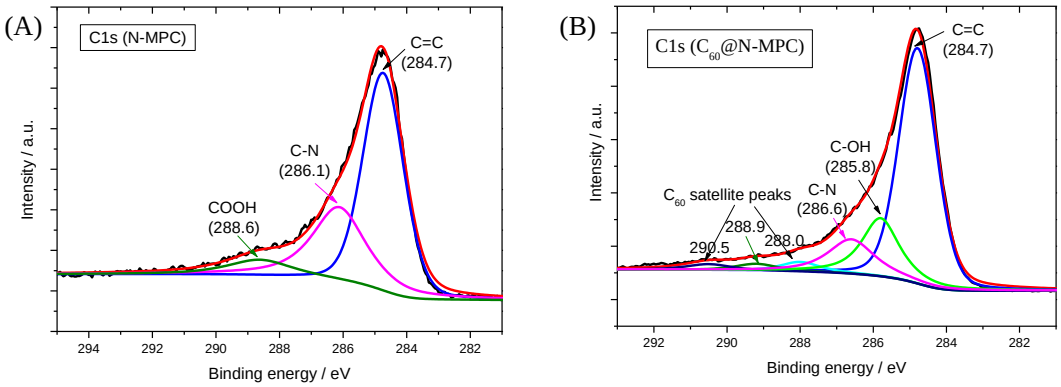

Figure S5. C1s XPS spectra of the unmodified N-MPC (A) and C_{60}@N-MPC (B). The two new peaks at 290.5 and 288.0 eV in the C1s XPS spectrum of C_{60}@N-MPC can be assigned to C1s shake-up satellite peaks of C_{60}.[S2]

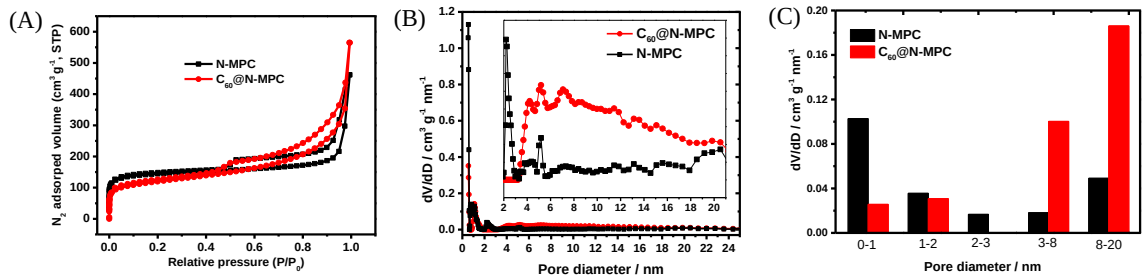

Figure S6. Nitrogen adsorption-desorption isotherms (A) and pore size distributions (B) of the unmodified N-MPC and C_{60}@N-MPC measured at 77 K. (C) Statistics of pore size distributions of the unmodified N-MPC and C_{60}@N-MPC.

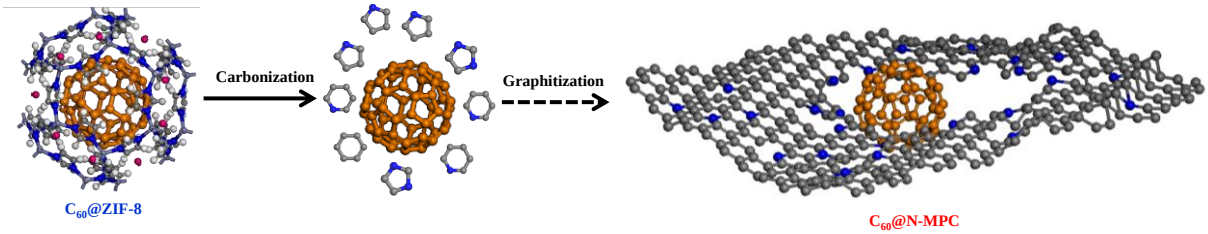

Figure S7. A schematic illustration of the formation of pores within C_{60}@N-MPC via carbonization of C_{60}@ZIF-8. In the existence of C_{60} molecules within some pores (diameter: ca. 1.1 nm[S3]) of ZIF-8, C_{60} may inhibit the direct transformation of such pores into new pores with comparable pore sizes within N-MPC, thus imposing the expanding of the pore size so as to accommodate the relatively large C_{60} molecules.

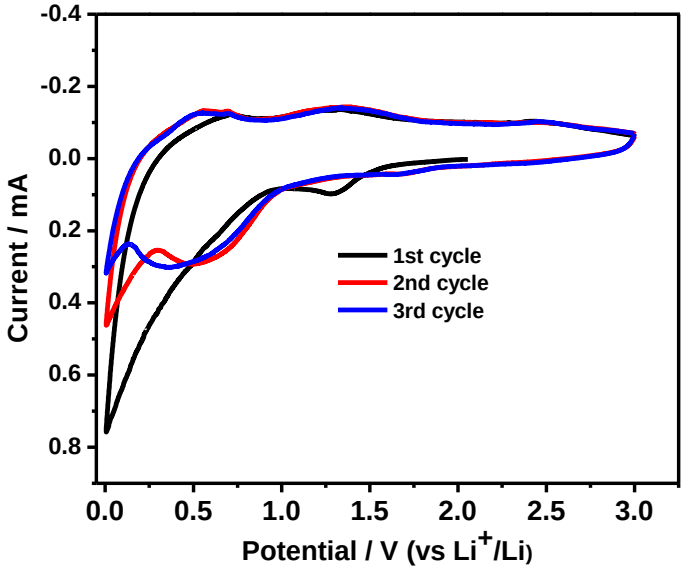

Figure S8. Cyclic voltammetric curve of the unmodified N-MPC at a scan rate of 0.2 mV s^{-1}.

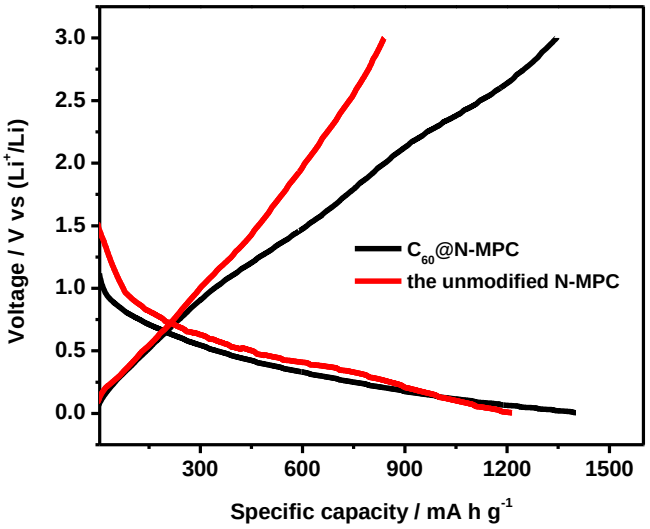

Figure S9. Voltage profiles of C_{60}@N-MPC and the unmodified N-MPC during the first cycle between 0.001 and to 3.0 V versus Li^+/Li at a cycling rate of 0.1 A g^{-1}. The capacities and current densities were calculated based on the masses of C_{60}@N-MPC and the unmodified N-MPC. The initial discharge and charge capacities of C_{60}@N-MPC are 2214 and 1443 mAh g^{-1}, respectively, both are much higher than that of the unmodified N-MPC (1214 and 839 mAh g^{-1}, respectively). The coulombic efficiencies of both anode materials are relatively low (≈ 65%), and this is probably due to the high surface contact area between carbon materials and the electrolyte.[S4]

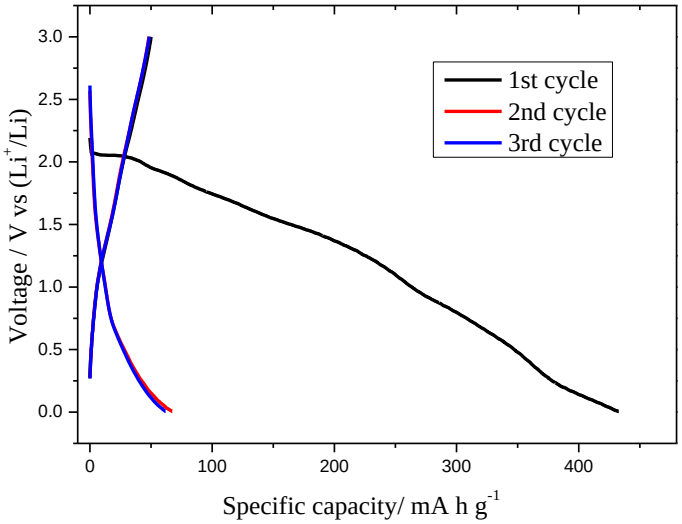

Figure S10. Voltage profile of C_{60} during the first three cycles between 0.001 and to 3.0 V versus Li^+/Li at a cycling rate of 0.1 A g^{-1}. The capacities and current densities were calculated based on the masses of C_{60}. The initial discharge and charge capacities of C_{60}@N-MPC are 435 and 50 mAh g^{-1}. The coulombic efficiencies is very low (≈ 11%).

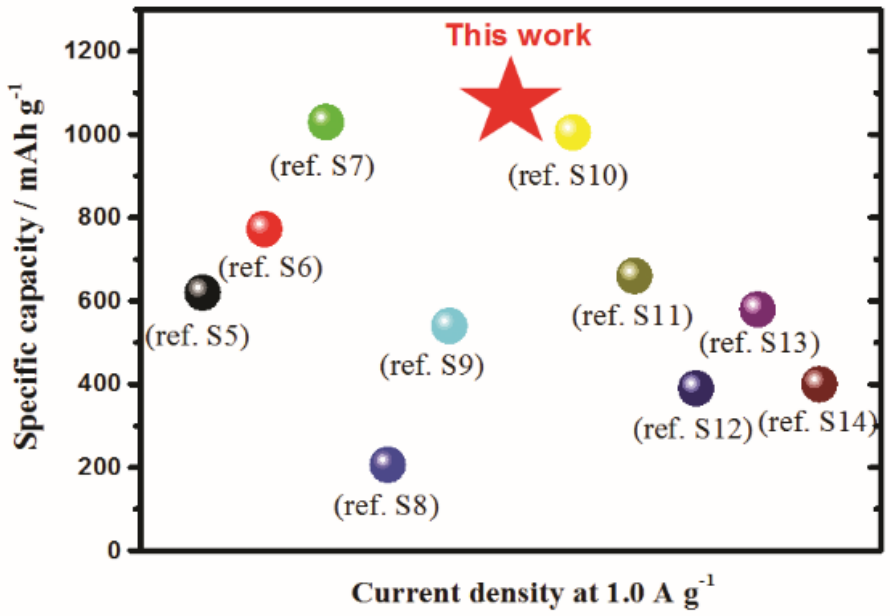

Figure S11. Comparison of the specific capacity of C_{60}@N-MPC in this work with those of most N-doped carbon materials reported in recent literatures. [S5-S14]

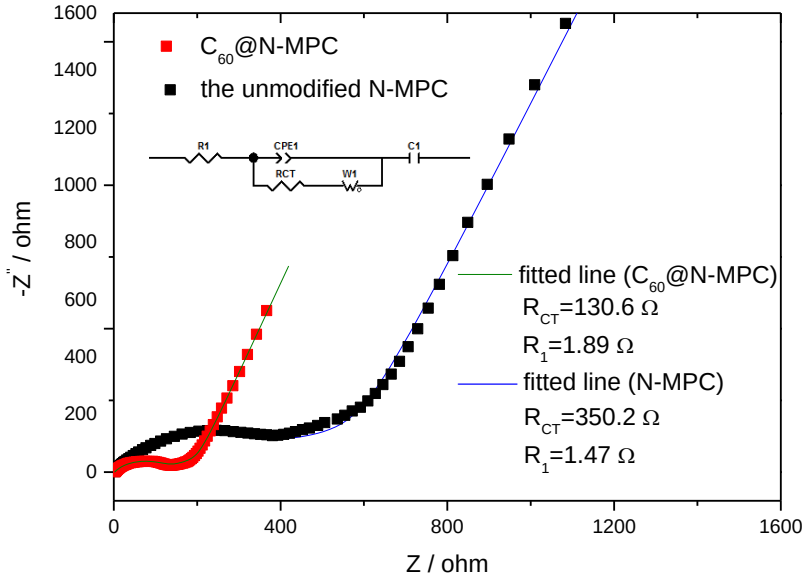

Figure S12. Nyquist plots of C_{60}@N-MPC and the unmodified N-MPC including the corresponding fitted curves based on the equivalent circuit model shown in the inset. Based on such an equivalent circuit model, two resistances including charge transfer resistance (R_{CT}) and electrolyte resistance (R1) can be obtained.[S15]

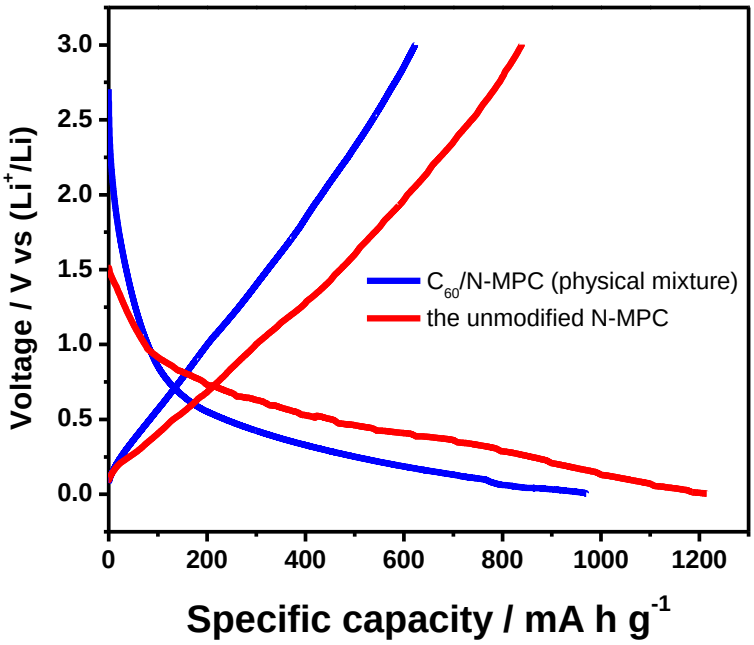

Figure S13. Voltage profiles of C_{60}/N-MPC (a physical mixture of C_{60} and N-MPC) and the unmodified N-MPC during the first cycle between 0.001 and to 3.0 V versus Li^+/Li at a cycling rate of 0.1 A g^{-1}.

References

S1. W. Chaikittisilp, M. Hu, H. Wang, H. –S. Huang, T. Fujita, K. C. W. Wu, L. C. Chen, Y. Yamauchi, K. Ariga, *Chem. Comm.*, 2012, **48**, 7259.

S2. C. Enkvist, S. Lunell, B. Sjögren, S. Svensson, P. A. Brühwiler, A. Nilsson, A. J. Maxwell, N. Mårtensson, *Phys. Rev. B*, 1993, **48**, 14629.

S3. Y. Han, P. Qi, X. Feng, S. Li, X. Fu, H. Li, Y. Chen, J. Zhou, X. Li. B. Wang, *ACS Appl. Mater. Interfaces*, 2015, **7**, 2178.

S4. F. Zheng, Y. Yang, Q. Chen, *Nat. Comm.*, 2014, **5**, 5261.

S5. L. Qie, W. M, Chen, Z. H, Wang, Q. G. Shao, X. L. X. Yuan, X. L. Hu, W. X. Zhang, Y. H. Huang, *Adv. Mater.*, 2012, **24**, 2047.

S6. P. Ramakrishnan, S. H. Baek, Y. Park, J. H. Kim, *Carbon*, 2017, **115**, 249.

S7. Z. Tan, K. Ni, G. Chen, W. Zeng, Z. Tao, M. Ikram, Q. Zhang, H. Wang, L. Sun, X. Zhu, X. Wu, H. Ji, R. S. Ruoff, Y. Zhu, *Adv. Mater.*, 2017, **29**, 1603414.

S8. X. Zhang, G. Zhu, M. Wang, J. Li, T. Lu, L. Pan, *Carbon*, 2017, **116**, 686.

S9. Z.-S. Wu, W. Ren, L. Xu, F. Li, H.-M. Cheng, *ACS Nano*, 2011, **5**, 5463.

S10. J. Hou, C. Cao, F. Idrees, X. Ma, *ACS Nano*, 2015, **9**, 2556.

S11. H. Wang, C. Zhang, Z. Liu, L. Wang, P. Han, H. Xu, K. Zhang, S. Dong, J. Yao, G. Cui, *J. Mater. Chem*., 2011, **21**, 5430.

S12. Z. Y. Sui, C. Wang, Q. S. Yang, K. Shu, Y. W. Liu, B. H. Han, G. G. Wallace, *J. Mater. Chem. A*, 2015, **3**, 18229.

S13. D. Zhou, X. Li, L. Z. Fan, Y. Deng, *Electrochim. Acta*, 2017, **230**, 212.

S14. L. Zhang, D. Ge, G. Qu, J. Zheng, X. Cao, H. Gu, *Nanoscale*, 2017, **9**, 5451.

S15. Z.-S. Wu, W. Ren, L. Xu, F. Li, H.-M. Cheng, *ACS Nano*, 2011, **5**, 5463.